Gyrotron Coaxial Cylindrical Resonators with Corrugated Inner Conductor: Theory and Experiment

Joaquim J. Barroso, Rafael A. Corrêa, and Pedro José de Castro

***Abstract*— Gyrotron coaxial resonators with a longitudinally slotted inner cylinder are examined analytically using a surface impedance model, from which expressions for the electromagnetic field, ohmic quality (Q) factor, and characteristic equation of the transverse eigenvalues $\chi_{m,p}$ are obtained. The major attributes of such resonators are expressed by the dependence of $\chi_{m,p}$ on the parameter C—defined as the ratio of the outer to inner radii of the coaxial structure. In that connection, the effect of the corrugation parameters on $\chi_{m,p}$ is particularly investigated on the basis of an expression derived for the slope function $d\chi_{m,p,p}/dC$. It is shown that the $\chi_{m,p}(C)$ curve may either exhibit oscillatory behavior or present a flat portion over a wide range of C depending on the corrugation parameters chosen. The theory is checked against experiment in which resonant frequencies and total Q factors were measured for TE modes operating in the range of 8–16 GHz in a coaxial cavity with 40 slots. Good agreement is found in that the magnitude of the relative error in frequency is less than 0.5%. Corrugated coaxial resonators proves to be relevant to megawatt gyrotrons where highly selective cavities are required to ensure high conversion efficiency.**

***Index Terms*— Corrugated coaxial cavities, gyrotron cavities, surface impedance model.**

I. Introduction

In THE development of high-power high-frequency gyrotrons, a major design constraint is the ohmic heating density of the cavity walls. To circumvent this problem, a very large (in the wavelength scale) overmoded cavity must be used in order to keep the ohmic losses at the acceptable limit of 3–4 kW/cm^2 for currently available cooling techniques. As the resonator cross section gets larger, the spectrum of eigenfrequencies becomes densely populated, leading to the possibility of mode interaction [1]. When simultaneous resonant interaction between several modes and the electron beam takes place, the gyrotron operation may be unstable. In addition, multimode oscillation causes a deterioration of the coherence and directivity of the generated radiation, gives rise to trapped modes and, in general, decreases the gyrotron efficiency.

An effective means in mode selection is provided by adjusting the electron-beam radius to ensure strong coupling between the operating TE_{mp} mode and the beam. However, as the gyrotron is scaled to megawatt powers at high frequency ($\sim$170 GHz) to meet the electron cyclotron resonance heating requirements for high-magnetic-field plasma configurations such as the international thermonuclear experimental reactor (ITER) [2], the spectrum of eigenmodes turns out so dense that it is necessary to employ still more precise methods of mode selection. Additional potentialities of rarefying the eigenfrequency spectrum as well as lowering the total quality (Q) factor of the competing modes can be achieved with the introduction of a coaxial insert into the open empty cylindrical resonator [3], [4]. Such a method of electrodynamic selection arises from the dependence of the transverse eigenvalues χ_{mp} upon the coaxial parameter C, defined as the ratio of the outer to inner radii of the coaxial resonator. Modes with close values of χ_{mp}, but distinct derivatives $d\chi_{mp}/dC$, will have diverse axial structures and, as result, different diffractive Q_D factors. It follows that an appropriate choice of the geometry of the inner conductor leaves the operating mode essentially unaffected by the presence of the insert, whereas potentially competing modes have their diffractive Q_D factors decreased.

Selective properties of coaxial cylindrical resonators can be further extended by the introduction of longitudinal corrugations on the inner conductor. Different from smooth coaxial cavities, a remarkable peculiarity of the function $\chi_{mp}(C)$, which results from the consideration of a corrugated inner wall, is the existence of extremes for circularly symmetric $\mathrm{TE}_{0,p}$ modes upon selecting suitable corrugation parameters, namely, the slot depth and corrugation period. Thus, corrugated coaxial cavities offer greater flexibility of handling mode-selection problems in gyrotron resonators. Although some useful design criteria have been given in previous works [5], [6], neither a more general consideration of corrugated coaxial cavities nor specific cold tests to validate the theory have yet been done.

In this paper, we make a systematic study of corrugated coaxial gyrotron cavities by examining the role played by the corrugation parameters in establishing the dependence of χ_{mp} on C. This question is addressed in Section II, where a surface-impedance model is used to describe the boundary conditions at the corrugated inner wall. An explicit expression for the slope function $d\chi_{mp}/dC$ is then obtained, which provides added insight into the selective properties of corrugated coaxial cavities. In Section III, taking into account the RF field inside the corrugation region, the energy-storage problem is studied, leading to an analytic formula for the ohmic Q factor. An experiment to verify the values of resonant frequency and total Q factor anticipated by theory is described

Manuscript received June 18, 1997; revised February 16, 1998.

The authors are with the Laboratory of Plasma, National Institute for Space Research (INPE), 12201-970 São José dos Campos, São Paulo, Brazil.

Publisher Item Identifier S 0018-9480(98)06168-7.

in Section IV, where measured and calculated results are compared. Section V contains the conclusions of our work.

II. Eigenvalues in Corrugated Coaxial Cylindrical Resonators

Let us consider a corrugated cylindrical cavity with geometry, as shown in Fig. 1, where the coaxial insert is a longitudinally slotted cylinder. Instead of using space harmonics [7] in the formulation of the electromagnetic-field problem, we shall proceed with a simpler method, usually referred to as the surface-impedance approach [8]. The method relies on the assumption that the ratio between the tangential $\overrightarrow{E}$ and $\overrightarrow{H}$ fields can be expressed as an impedance-type boundary condition, and that such a ratio must be given unambiguous in terms of the geometry of the corrugated wall. Under the condition that the slot width is less than a half-wavelength of the operating mode, which means that the field variation along a slot interval in negligible, the corrugations may be represented by a homogeneous reactive surface at $r = R_i$ (see Fig. 1). The approximation improves as the number of slots per wavelength increases and the thickness of the ridge decreases. Therefore, when space harmonics are neglected, the field components for TE_{mp} modes in the annular region are those in a coaxial guide with smooth walls

$$E_\phi = \frac{\partial \Psi_{mp}(r,\phi)}{\partial r} V(z) \tag{1a}$$

$$E_r = -\frac{1}{r}\frac{\partial \Psi_{mp}(r,\phi)}{\partial \phi} V(z) \tag{1b}$$

$$H_z = \frac{-i}{\omega\mu_0} k_\perp^2 \Psi_{mp}(r,\phi) V(z) \tag{1c}$$

where $\Psi_{mp}(r,\phi) = A_{mp}\mathcal{C}_m(k_\perp r)e^{im\phi}$ with the cylinder function of order m

$$\mathcal{C}_m(k_\perp r) = J_m(k_\perp r)Y'_m(k_\perp R_0) - Y_m(k_\perp r)J'_m(k_\perp R_0) \tag{2}$$

where J_m and Y_m are, respectively, Bessel functions of the first and second kinds with primes denoting differentiation with respect to the argument; A_{mp} is a normalization parameter to be determined in Section III, $V(z)$ is a function expressed in volts describing the longitudinal profile of the fields, and $k_\perp = \chi_{mp}/R_0$ is the transverse eigenvalue. We have assumed a harmonic variation $e^{i\omega t}$ for the electromagnetic field.

Provided that $l < \lambda/2$, there is no azimuthal propagation of energy inside the slots, as high-order TE modes are below cutoff. Thus, we shall take in the slots only the lowest order TE mode, which has the following components:

$$e_\phi = -k_\perp \Psi_{mp}(k_\perp R_i) \cdot \frac{J_1(k_\perp r)Y_1(k_\perp R_d) - Y_1(k_\perp r)J_1(k_\perp R_d)}{J_0(k_\perp R_i)Y_1(k_\perp R_d) - Y_0(k_\perp R_i)J_1(k_\perp R_d)} \cdot V(z)e^{i(2\pi/N)qm} \tag{3a}$$

$$h_z = \frac{-ik_\perp^2}{\omega\mu_0}\Psi_{mp}(k_\perp R_i) \cdot \frac{J_0(k_\perp r)Y_1(k_\perp R_d) - Y_0(k_\perp r)J_1(k_\perp R_d)}{J_0(k_\perp R_i)Y_1(k_\perp R_d) - Y_0(k_\perp R_i)J_1(k_\perp R_d)} \cdot V(z)e^{i(2\pi/N)qm} \tag{3b}$$

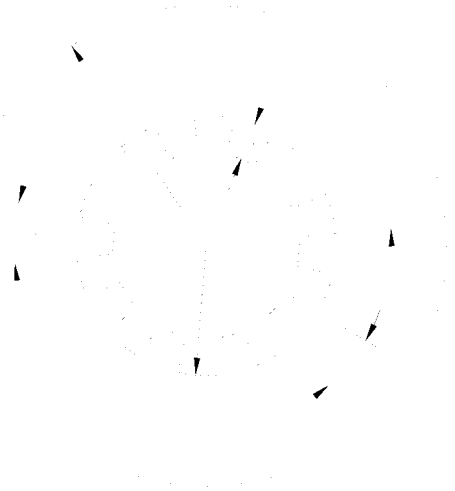

Fig. 1. Cross section of a corrugated coaxial cylindrical cavity. (The corrugation period s, slot width l, number of slots N, and slot angle $2\theta_s$ are related by $N\theta_s/\pi = l/s$.)

$$h_r = -\frac{i}{\omega\mu_0}\frac{\partial e_\phi}{\partial z} \tag{3c}$$

where N denotes the number of slots and q is the slot index. In the wall reactance model, it is assumed that e_ϕ across each slot is constant and, further, that the field at any slot differs from the field at a neighboring slot only by a constant phase factor $e^{i(2\pi/N)qm}$, with the total phase shift around the periodic structure being a multiple of 2π (Floquet's theorem). Notice in (3a) that $e_\phi = 0$ at $r = R_d$.

The characteristic equation for the transverse wavenumber is obtained by applying continuity conditions to the surface reactance at $r = R_i$. Thus, the reactance X looking into the interaction space from the slots across the boundary is matched to the reactance viewed from interaction space and averaged around the circumference at $r = R_i$

$$-\frac{E_\phi}{H_z} = iX = -\left\langle \frac{e_\phi}{h_z} \right\rangle. \tag{4}$$

Then, using (2)–(4) and letting $k \simeq k_\perp$ as gyrotron resonators operate close to cutoff, we obtain at $r = R_i$

$$\mathcal{C}'_m(k_\perp r)|_{r=R_i} = -\langle w_s \rangle \mathcal{C}_m(k_\perp r)|_{r=R_i} \tag{5}$$

where $w_s = i(e_\phi/h_z)/\sqrt{\mu_0/\epsilon_0}|_{r=R_i}$ is a surface reactance normalized to the impedance of free space and

$$\langle w_s \rangle = \frac{1}{2\pi}\int_0^{2\pi} w(\phi)\, d\phi \tag{6}$$

where

$$w(\phi) = \begin{cases} w_s, & \dfrac{2\pi q}{N} - \theta < \phi < \dfrac{2\pi q}{N} + \theta \\ 0, & \text{for all other values of } \phi \end{cases}$$

with 2θ denoting the slots angle. In this way, the corrugated surface is represented in terms of a surface boundary condition involving only the interaction space fields, thereby converting a two-media problem into a single one.

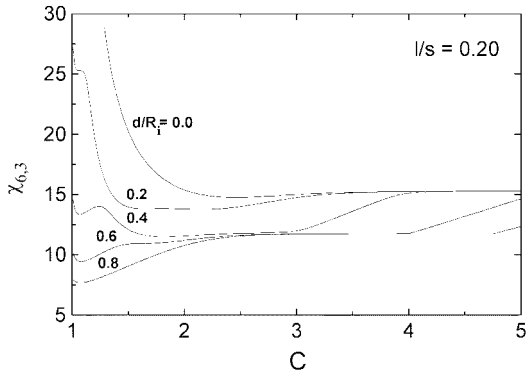

Fig. 2. $\mathrm{TE}_{6,3}$—mode eigenvalue $\chi(C)$ curves with d/R_i as parameter.

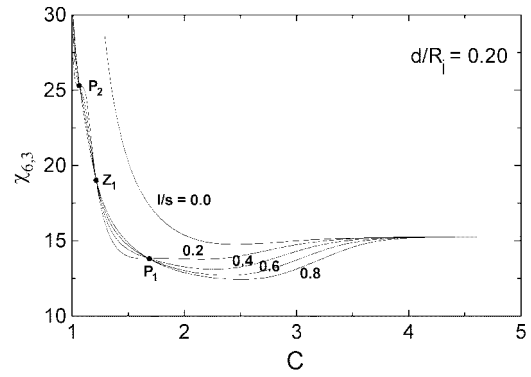

Fig. 3. $\mathrm{TE}_{6,3}$—mode eigenvalue $\chi(C)$ curves with l/s as parameter.

Noting that $\langle w_s \rangle = (l/s)w_s$, (5) is rewritten as

$$\frac{J'_m(x)Y'_m(y) - J'_m(y)Y'_m(x)}{J_m(y)Y'_m(x) - J'_m(x)Y_m(y)} = \frac{l}{s}\,\frac{J_1(y)Y_1(y_d) - Y_1(y)J_1(y_d)}{J_0(y)Y_1(y_d) - Y_0(y)J_1(y_d)} \quad (7)$$

which gives the characteristic equation for the transverse eigenvalues $\chi_{mp} = k_\perp R_0 \equiv x$, where $y \equiv \chi_{mp}/C$ with $C = R_0/R_i$ and $y_d = y(1 - d/R_i)$.

To examine the effects of the corrugation parameters, namely, the relative slot-depth d/R_i and the parameter l/s defined as the slot-opening l normalized to the ridge-slot period s (Fig. 1), we plot in Figs. 2 and 3 the $\mathrm{TE}_{6,3}$-mode eigenvalue curves $\chi(C)$ having, respectively, d/R_i and l/s as parameters. Firstly, we see that the $\chi(C)$ curves are shifted downward relative to the eigenvalue curves for the smooth-wall case $(d/R_i = 0)$. This means that the cutoff frequency is decreased since the electric field penetrates into the slot region, thus increasing the resonating volume. This is similar to the ohmic effect in a smooth cavity, in which a resonant frequency in a lossy cavity is always less than in a cavity with perfectly conducting walls.

Secondly, different from the smooth-wall case, for which the eigenvalue increases without limit as $C \to 1$, a noticeable effect is that the eigenvalue for the corrugated cavity is limited as $C \to 1$. This limiting value can be easily estimated by noting that as $C \longrightarrow 1$, the numerator of the right-hand side of (7) tends to zero. Then, we must have $w = 0$, i.e., $J_1(\chi_{mp})Y_1(\chi_{mp}(1-d/Ri)) - Y_1(\chi_{mp}(1-d/Ri))J_1(\chi_{mp}) = 0$. Using the asymptotic forms of Bessel and Neumann functions for large arguments, we arrive at $\sin(\chi_{mp}d/R_i) = 0$ or $\chi_{mp} = (p-1)\pi/(d/R_i)$ where p is an integer denoting the radial-mode number. For $p = 3$ and $d/R_i = 0.4$, we see that $\chi_{6,3} \simeq 5\pi$ at $C = 1$, as shown in Fig. 2. The mode propagating radially in the annular-sector resonator strongly resembles the TE_{10} mode of the rectangular guide, although modified by the convergence of the slot sides.

We also note in Fig. 3 that all the curves intersect regularly at some points and, moreover, for $l/s = 0.2$, the $\chi(C)$ curve flattens with its slope approaching zero at the intersection point P_1. To investigate the effect on the $\chi(C)$ curve shape, varying the corrugation parameters, we shall look at the extremes of the eigenvalue curves. By expressing the derivative of $\chi_{m,p}$ with respect to C in the form

$$\frac{d\chi}{dC} = -\frac{\partial F/\partial C}{\partial F/\partial x} \quad (8)$$

where

$$\begin{aligned} F(x, C) &= Y'_m(x)J'_m(y) - J'_m(x)Y'_m(y) \\ &\quad + w[J_m(y)Y'_m(x) - J'_m(x)Y_m(y)] \\ &= 0 \end{aligned} \quad (9)$$

with

$$w = \frac{l}{s}\,\frac{J_1(y)Y_1(y_d) - Y_1(y)J_1(y_d)}{J_0(y)Y_1(y_d) - Y_0(y)J_1(y_d)} \quad (10)$$

we arrive at

$$\frac{d\chi_{mp}}{dC} = \frac{\chi_{mp}}{C}\,\frac{-f(y)}{(x^2 - m^2)\left[\dfrac{wJ_m(y) + J'_m(y)}{CJ'_m(x)}\right]^2 - f(y)} \quad (11)$$

where

$$f(y) = y^2w^2\left(1 - \frac{s}{l}\right) + y^2\left(1 - \frac{s}{l}\right) + \frac{l}{s}\,y_d^2G^2(y_d) - m^2 \quad (12)$$

with

$$y_dG(y_d) = \frac{4/\pi}{J_1(y_d)Y_0(y) - J_0(y)Y_1(y_d)}. \quad (13)$$

As will be shown in Section III, the denominator of the right-hand side of (11) is always positive. Hence, the sign of the derivative $d\chi/dC$ is opposite to the sign of $f(y)$ and, further, the condition for obtaining an extremum of $\chi(C)$ is given by $f(y) = 0$. To illustrate this point, we show in Fig. 4 the function $yf(y)$ corresponding to the corrugation parameters $d/R_i = 0.4$, $l/s = 0.2$, and azimuthal number $m = 6$. The zeros of $yf(y)$ are assigned by the labels from A to F and, for comparison purposes, the dashed curve represents the function in the smooth-wall case $(w = 0)$. Examining this plot, we can anticipate the behavior of the eigenvalue curves for the family

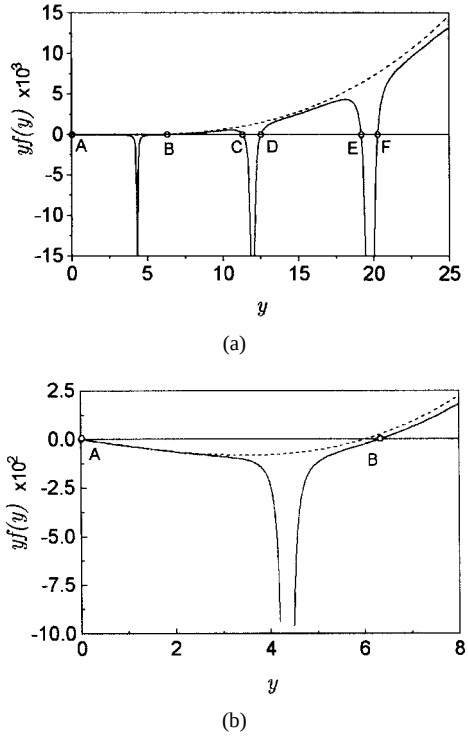

Fig. 4. (a) Function $yf(y)$ associated with corrugation parameters $d/R_i = 0.4$, $l/s = 0.2$, and azimuthal number $m = 6$. (The corresponding zeros are labeled from A to F and the dashed line represents the function for the smooth wall case ($w = 0$). The plots are shown in greater detail in (b), where the second zero labeled as B is shifted to higher y values relative to the $w = 0$ case.)

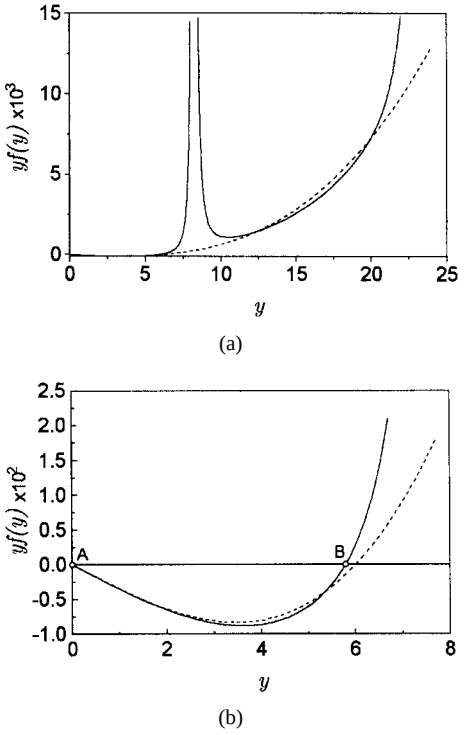

Fig. 5. (a) Function $yf(y)$ associated with corrugation parameters $d/R_i = 0.2$, $l/s = 0.4$, and azimuthal number $m = 6$. (The dashed line represents the function for the smooth wall case ($w = 0$). For these corrugation parameters, the function possesses only two zeros and, as shown in (b), the second zero is shifted to lower y values relative to the $w = 0$ case.)

of modes $\mathrm{TE}_{6,p}$ with radial number $p > 1$. As the variable y is the ratio of eigenvalue χ to parameter C, the first zero at $y_A = 0$, shown in the expanded plot of Fig. 4(b), implies that the eigenvalue curves tend asymptotically to $C \to \infty$ with zero $d\chi/dC$ slope. This limit corresponds to the hollow cylindrical resonator for which the determinantal equation (9) reduces to $J'_m(x) = 0$.

Since $yf(y) < 0$ in the range $y_A < y < y_B$, as shown in Fig. (4), the slope $d\chi/dC$ is positive in this range with $y_B = 6.31$ corresponding to the first local minimum on the $\chi(C)$ curve. From y_B to y_C, the derivative $d\chi/dC$ is negative and $y_C = 11.29$ should correspond to a local maximum. Further, $y_D = 12.51$ gives a minimum, $y_E = 19.17$ is a maximum, and so on. For this case, we may infer, therefore, without solving the characteristic equation (9), that the function $\chi(C)$ has an oscillatory behavior with alternating minima and maxima, with the oscillation period shortening as y increases. On the other hand, the function $yf(y)$ displays a different behavior when the following corrugation parameters $d/R_i = 0.20$ and $l/s = 0.40$ are considered. In this case [see Fig. 5(a)], there exists only one minimum; after reaching this minimum at $y = 5.79$ [see Fig. 5(b)] the curves $\chi_{6,p}(C)$ with $p > 1$ should exhibit negative slope.

We can obtain still more information about the eigenvalue curves $\chi(C)$ by noting in Figs. 4 and 5 that the function $yf(y)$ diverges as $|w|$ goes to infinity. Upon using the asymptotic forms of Bessel and Neumann functions for large arguments in (10), we have $w = (l/s), \tan(y_d/R_i)$ and (11) reduces to

$$\frac{d\chi_{mp}}{dC} = \frac{\chi_{mp}}{C} \frac{-\left(1 - \dfrac{d/R_i}{l/s}\right)}{\dfrac{x^2 - m^2}{x^2} \dfrac{J_m^2(y)}{J_m'^2(x)} - \left(1 - \dfrac{d/R_i}{l/s}\right)} \tag{14}$$

as $|w| \to \infty$. Recalling that the denominator of the right-hand side of (14) is positive, we see for $(d/R_i)/(l/s) > 1$ that the derivative $d\chi/dC$ is positive and, accordingly, $yf(y)$ diverges to minus infinity, as shown in Fig. 4; the converse occurs for $(d/R_i)/(l/s) < 1$ and, as $|w| \to \infty$, the limiting value of $yf(y)$ is $+\infty$, as shown in Fig. 5. In the particular case when $(d/R_i)/(l/s) = 1$, we have $d\chi/dC = 0$ associated with the singular points of $f(y)$.

Now considering the corrugation parameters $d/R_i = 0.4$ and $l/s = 0.2$, shown in Fig. 6, we examine the eigenvalue curves of modes $\mathrm{TE}_{6,p}$ with radial indices ranging from $p = 1$ to $p = 4$. The dashed straight lines, labeled from y_B to y_F, are drawn with slopes that correspond to the zeros of $yf(y)$ in Fig. 4. If we make a correlation between these plots, it is apparent that the first minimum of the $\chi(C)$ curves lies on $y = y_B$, whereas the first local maxima are joined by $y = y_C$.

In Fig. 7, we plot the eigenvalue curves for $\mathrm{TE}_{6,p}$ modes considering $d/R_i = 0.20$ and $l/s = 0.40$, which yield only one point of minimum (for $p > 1$), as had been anticipated by Fig. 5. By contrast, for $d/R_i = l/s = 0.4$, we see in Fig. 8 that the $\mathrm{TE}_{6,4}$-mode curve broadens and flattens over a relatively large range of the parameter C. In this particular case, the singular points of $f(y)$ are associated with a zero-

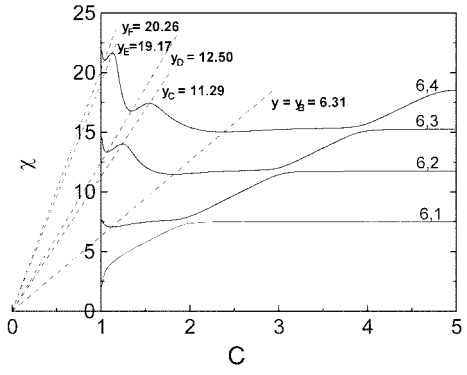

Fig. 6. Eigenvalue curves for modes $\mathrm{TE}_{6,\,p}$ with $1 \leq p \leq 4$ in a corrugated coaxial cavity where $d/R_i = 0.40$ and $l/s = 0.20$. (The angular coefficient of the dashed straight lines $y = \chi/C$ correspond to the zeros of the function $f(y)$.)

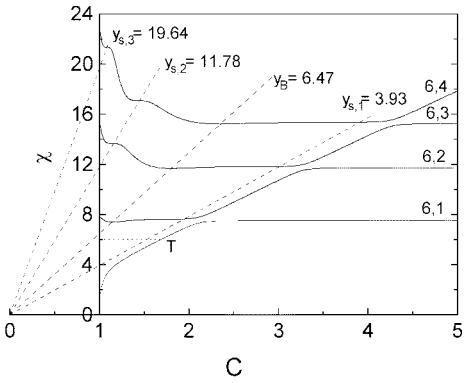

Fig. 8. Eigenvalue curves for modes $\mathrm{TE}_{6,\,p}$ with $1 \leq p \leq 4$ in a corrugated coaxial cavity with $d/R_i = l/s = 0.40$. (The dashed straight lines $y = \chi/C$ are drawn with angular coefficients y_B and $y_{s,\,p}$, which correspond to the first zero and the singular points of the function $f(y)$.)

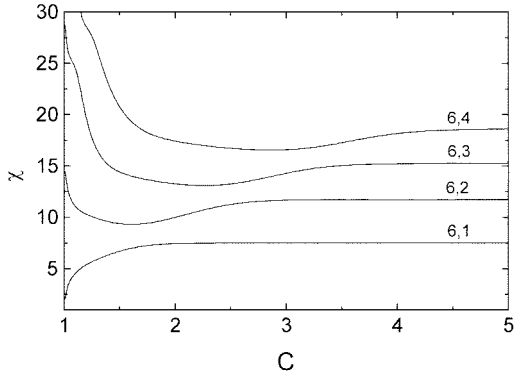

Fig. 7. Eigenvalue curves for modes $\mathrm{TE}_{6,\,p}$ in a corrugated coaxial cavity with $d/R_i = 0.20$ and $l/s = 0.40$. (In this case, the curves with $p > 1$ exhibit only one minimum.)

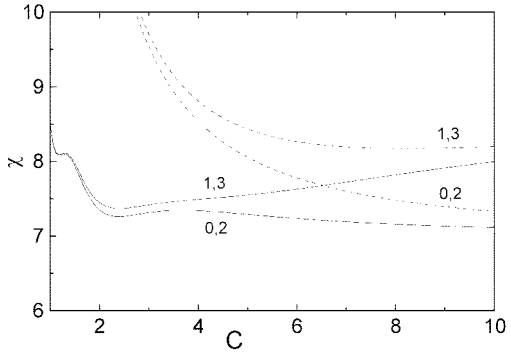

Fig. 9. Eigenvalue curves for modes $\mathrm{TE}_{0,\,2}$ and $\mathrm{TE}_{1,\,3}$ in a corrugated coaxial cavity with $d/R_i = l/s = 0.75$. (The dashed curves refer to the smooth coaxial cavity.)

derivative $d\chi/dC$, as pointed out by (14); therefore, all the $\chi(C)$ curves have zero slope when crossing the line $y = y_{s,\,1}$ corresponding to the first singular point at $y_{s,\,1} \simeq 1.25\pi$, which explains the flatness of the main portion $y_B \geq y \geq y_{s,\,1}$ of the curves. For $y \gg 1$, the singular points of $f(y)$, or the poles of w are approximated by $y_{s,\,p} = (2p-1)\pi/(2d/R_i)$, and it is apparent that the upper curves $\chi_{6,\,4}$ and $\chi_{6,\,3}$ exhibit secondary plateaus in the neighborhood of the intersection points on the lines $y = y_{s,\,2} = 3.75\pi$ and $y = y_{s,\,3} = 6.25\pi$. Moreover, for $w = 0$ or $|w| \to \infty$ the characteristic equation (9) reduces, respectively, to $Y'_m(y)J'_m(x) - J'_m(y)Y'_m(x) = 0$ or $J'_m(x)Y_m(y) - J_m(y)Y'_m(x) = 0$, thus implying that the eigenvalue of a given TE mode becomes independent of the corrugation parameters in these limiting cases. We can conclude, therefore, that the alternate intersection points P and Z in Fig. 3 correspond to the poles and zeros of w, respectively. We also see in Fig. 8 that the $y_{s,\,1}$ line does not intercept the $\mathrm{TE}_{6,\,1}$-mode curve. Such a lowest order mode with circumferential variations is very insensitive to the presence of the corrugated rod and has a unique feature in exhibiting transverse eigenvalues lower than the azimuthal number $m = 6$. This yields that the tangent to the curve $\chi_{6,\,1}$ through the point T (corresponding to $\chi = 6$) coincides with the line connecting this point and the origin at $C = 0$ since, according to (14), $d\chi/dC = \chi/C$ for $m = \chi$.

We conclude this section by highlighting the potentialities of mode selection in corrugated coaxial cavities. Considering the corrugation parameters $d/R_i = l/s = 0.75$, the eigenvalue curves for the modes $\mathrm{TE}_{0,\,2}$ and $\mathrm{TE}_{1,\,3}$ take on the form shown in Fig. 9, where the slopes of the curves at $C = 5$ have opposite signs. Thus, if a downtapered rod (i.e., narrowing to the cavity output) with average radius $R_i = R_0/5$ is used, then the $\mathrm{TE}_{0,\,2}$-mode diffractive factor Q can be greatly enhanced [3]–[5] relative to that of the competing mode $\mathrm{TE}_{1,\,3}$. Such a method can be employed in highly overmoded cylindrical cavities so as to provide an effective mode selection in megawatt gyrotrons.

III. Energy Storage and Ohmic Q Factor

The ohmic Q factor of a resonator gives a measure of the power dissipated in the conducting walls and is determined

by calculating the time-averaged energy $\mathcal{E}$ stored in the cavity and then evaluating the average power dissipated P_d into the walls, i.e.,

$$Q_\Omega = \frac{\omega_0 \mathcal{E}}{P_d} \tag{15}$$

where ω_0 is the angular frequency of the field, assuming no losses. The stored energy is written in the form

$$\mathcal{E} = \frac{\epsilon_0}{2} \int_0^L |V(z)|^2 \, dz \int_A |E(r, \phi)|^2 \, dA \tag{16}$$

with L and A denoting the length and cross-section area of the cavity, respectively. In evaluating the surface integral, the interaction space and slot region are considered separately; then, substituting the expressions given in (1) and (3) for the electric fields, the result is

$$\begin{aligned}\int_A |E(r, \phi)|^2 \, dA &= \pi A_{mp}^2 \Bigg\{ (x^2 - m^2) \mathcal{C}_m^2(x) \\ &\quad - ((y^2 - m^2) + w^2 y^2 - 2yw) \mathcal{C}_m^2(y) + y^2 \mathcal{C}_m^2(y) \\ &\quad \cdot \left[\frac{s}{l} w^2 - 2 \frac{w}{y} + \frac{s}{l} \left(1 - \frac{y_d^2}{y^2} G^2(y_d) \right) \right] \Bigg\} \end{aligned} \tag{17}$$

where the contribution arising from the slot resonators is represented by the last term in brackets. The currents flowing in the metal walls generate the ohmic power loss $P_d = (R_s/2) \int |\overrightarrow{H_{\tan}}|^2 \, dA$ where $R_s = \omega_0 \mu \delta / 2$ is the surface resistivity and $\delta = (2/\omega \mu \sigma)^{1/2}$ is the skin depth with σ denoting the conductivity of the metal. Substituting the axial magnetic field components given in (1c) for the interaction region and in (3b) for the slot region, and neglecting the transverse magnetic-field components since the gyrotron operates close to cutoff, i.e., $k_\parallel \ll k_\perp$, we get (18), shown at the bottom of this page, where the terms in brackets give the power lost by the inner rod, i.e., on the top wall, base wall, and sidewall of the slots, respectively; η is the impedance of free space and $R_{s,0}$ and $R_{s,i}$ indicate the surface resistivity of the outer and inner walls. If we normalize to unity the integral on the left-hand side of (17), and substitute (17) and (18) in (15), an expression for the ohmic Q factor is obtained, as shown in (19), at the bottom of this page, where $\langle G^2(y_d) \rangle = (1/k_\perp d) \int_{y_d}^{y} G^2(y) \, dy$ and the normalization factor A_{mp} is expressed by (20), shown at the bottom of this page. Note that the term in brackets is exactly the function $f(y)$ as defined in (12), i.e.,

$$A_{mp}^{-2} = \pi \{ (x^2 - m^2) \mathcal{C}_m^2(x) - \mathcal{C}_m^2(y) f(y) \}. \tag{21}$$

As an illustration of these relations, we consider a cavity with external guide of radius $R_0 = 3.4$ cm and inner rod with corrugation parameters $d/R_i = 0.5$ and $l/s = 0.25$ and $N = 36$ slots; conductivities of $\sigma_0 = 3.8 \times 10^7$ S/m (copper) and $\sigma_i = 2.5 \times 10^7$ S/m (aluminum) are assumed for the outer and inner cylinders, respectively. For this cavity, the transverse eigenvalue of the mode $\mathrm{TE}_{1,5}$, its associated Q_Ω factor, and the normalization parameter πA_{mp}^{-2} are shown as a function of the coaxial variable C in Fig. 10. The points $B, C, \cdots, H$ lying on the $\chi(C)$ curve correspond to the zeros of $f(y)$, and the interlaced points labeled as $w = 0$ or $w = \infty$ are those at which the reactance w has a zero or a pole. In Fig. 10, we first see that both Q_Ω and πA_{mp}^{-2} are oscillatory functions of C with the maxima on the πA_{mp}^{-2} curve correlating with the $w = \infty$ points. In fact, since $\chi \gg m$ and noting that $\mathcal{C}_m(x) = 2/(\pi x)$, (21) can be rewritten as $\pi A_{mp}^{-2} \simeq 4 - \pi^2 \mathcal{C}_m^2(y) f(y)$; thus the zeros of $f(y)$ give a value of about four for the normalization parameter, as indicated by the dotted line in Fig. 10. Now letting $y \gg 1$ and taking the limit as $|w| \to \infty$, the last equation yields

$$\begin{aligned}\pi A_{mp}^{-2} = 4 - \pi^2 &\left(1 - \frac{d/R_i}{l/s} \right) \\ &\cdot \{ y [J_m'(x) Y_m'(y) - J_m'(y) Y_m'(x)] \}^2. \end{aligned} \tag{22}$$

Therefore, since in our example $d/R_i > l/s$, a maximum for πA_{mp}^{-2} occurs around $w = \infty$ when $y \gg 1$. Even though the axial magnetic-field component h_z, as given in (3b), is zero on the corrugated top surface at $r = R_i$ when $|w| \to \infty$, the corresponding Q_Ω factors attain the lowest values; in this condition, the slot depth is about equal to a quarter-wavelength (since $w = (l/s) \tan k_\perp d$ in the approximation $y \gg 1$) and,

$$P_d = \pi A_{mp}^2 \frac{k_\perp^2}{\eta^2} \int_0^L |V(z)|^2 \, dz \Bigg\{ R_{s,0} R_0 \mathcal{C}_m^2(x) + R_{s,i} \mathcal{C}_m^2(y) \left[R_i \left(1 - \frac{l}{s} \right) + (R_i - d) \frac{l}{s} G^2(y_d) + N \int_{R_i - d}^{R_i} G^2(k_\perp r) \, dr \right] \Bigg\} \tag{18}$$

$$Q_\Omega = \frac{R_0}{\delta_0} \frac{A_{mp}^2/(\pi x^2)}{\mathcal{C}_m^2(x) + \frac{\delta_i}{\delta o} \frac{\mathcal{C}_m^2(y)}{C} \left[\left(1 - \frac{l}{s} \right) + \left(1 - \frac{d}{R_i} \right) + \frac{l}{s} G^2(y_d) + \frac{N}{\pi} \frac{d}{R_i} \langle G^2(y_d) \rangle \right]} \tag{19}$$

$$A_{mp}^{-2} = \pi \left\{ (x^2 - m^2) \mathcal{C}_m^2(x) - \mathcal{C}_m^2(y) \left[(y^2 - m^2) + w^2 y^2 - y^2 \left(\frac{s}{l} w^2 + \frac{l}{s} \left(1 - \frac{y_d^2}{y^2} G^2(y_d) \right) \right) \right] \right\} \tag{20}$$

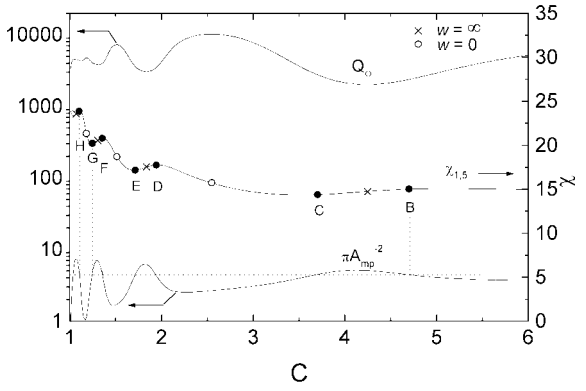

Fig. 10. Ohmic Q_Ω factor, normalization parameter πA_{mp}^{-2}, and transverse eigenvalue as function of the coaxial variable C for the $\mathrm{TE}_{1,5}$ mode operating in a cavity with $R_0 = 3.4$ cm and corrugation parameters $d/R_i = 0.50$, $l/s = 0.25$, and $N = 36$ slots. (Conductivities of $\sigma_0 = 3.8 \times 10^7$ S/m (copper) and $\sigma_0 = 2.5 \times 10^7$ S/m (aluminum) are assumed for the outer and inner cylinders, respectively.)

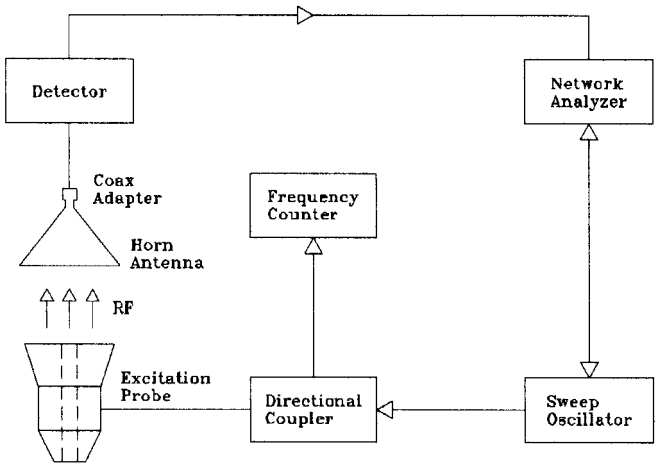

Fig. 11. Schematic of the cold-test measurement apparatus.

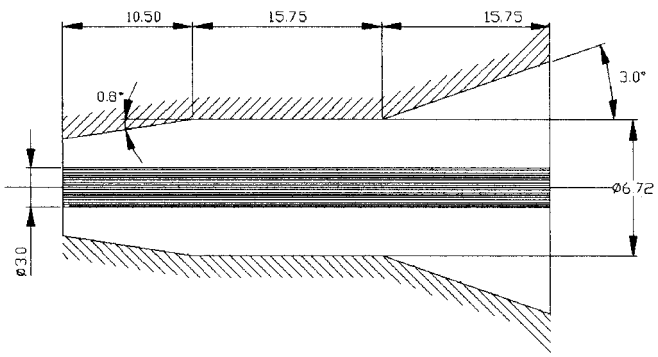

Fig. 12. Schematic diagram (dimensions in centimeters) of the corrugated coaxial resonator tested. (Corrugation parameters are $l/s = 0.42$, $d/R_i = 0.10$, and $N = 40$ slots.)

accordingly, the dissipated power in the inner rod arises from the bottom and side surfaces of the slots. On the other hand, the slot, in the sense of a short-circuited transmission line, acts as a resonant circuit when $w = 0$, thus giving the highest Q_Ω factors (see Fig. 10).

Finally, combining the term $wJ_m(y) + J'_m(y)$ in brackets on the right-hand side of (11) with the characteristic equation (9) gives

$$\frac{wJ_m(y) + J'_m(y)}{CJ'_m(x)} = \frac{\mathcal{C}_m(x)}{\mathcal{C}_m(y)}. \tag{23}$$

Substituting this result in (11) and using (21), the slope function $d\chi/dC$ is recast in compact form as

$$\frac{d\chi}{dC} = -\pi A_{mp}^2 y f(y) \mathcal{C}_m^2(y) \tag{24}$$

with $y = \chi/C > 0$. This proves that $d\chi/dC$ and $yf(y)$ have opposite signs, as previously discussed in Section II.

IV. Experiment and Comparison with Theory

A. Description of the Experiment

A schematic diagram of the experimental setup is shown in Fig. 11. The source of probing radiation was a sweep oscillator incorporated into a network analyzer, which provided transmission measurements in the examined frequency range from 8 to 16 GHz. TE modes were excited by means of an electric probe introduced into a 2.0-mm-diameter hole drilled in the midsection of the outer guide. To collect the power reradiated by the quasi-stationary field, a pyramidal horn antenna connected to a detector was placed in front of the output section of the cavity. For each mode under observation, the exciting probe and receiving antenna were properly oriented so that the observed resonance curve on the network analyzer display could be symmetrical and as narrow as possible. The Q measured was the total Q as directly determined from frequency readings at the half-points on the detected spectrum.

The outer structure of the coaxial cavity (see Fig. 12) is a weakly irregular guide which comprises a straight cylindrical section joined to two linear tapers. Notice that the taper angles are made small (<5°) so that we ignore the conversion of a waveguide wave into other wave modes upon its reflection from the critical cross section. An electro-forming technique was used to fabricate the outer guide in a single copper piece for which an electrical resistivity of $\sigma_0 = 3.8 \times 10^7$ S/m has been assumed. The corrugated inner conductor is a 3.00-cm-diameter cylinder made of aluminum ($\sigma_i = 2.5 \times 10^7$ S/m) with corrugation parameters $d/R_i = 0.10$, $l/s = 0.42$, and $N = 40$ slots.

B. Calculation of Resonant Frequency and Total Q Factor

Assuming single-mode approximation, resonant frequency, and diffractive Q factor (Q_D) are determined from the complex eigenfrequency $f = f_R + if_I$, which renders the equation for the longitudinal distribution $V(z)$ of the electromagnetic [4]

$$\frac{d^2V(z)}{dz^2} + (4\pi^2 f^2/c^2 - k_{\perp,mp}^2)V(z) = 0 \tag{25}$$

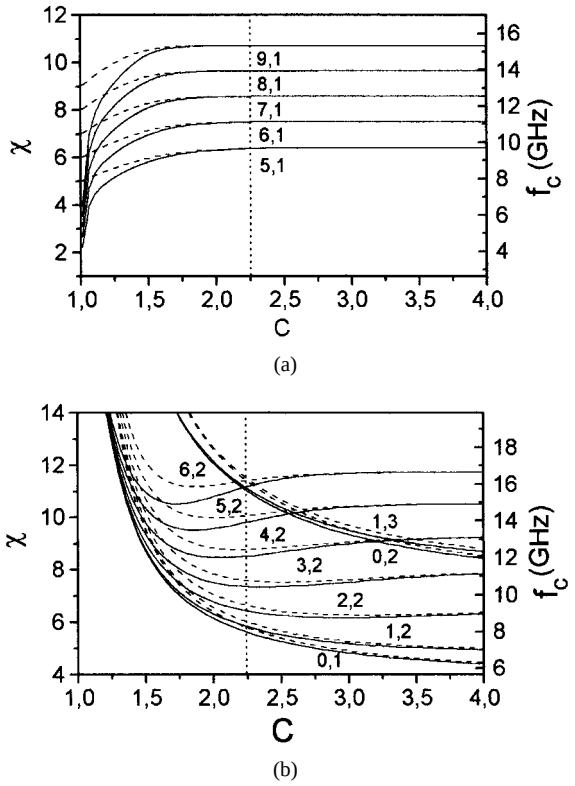

Fig. 13. Dependence of transverse eigenvalue $\chi_{m,p}$ on coaxial parameter C for (a) surface and (b) volume $\mathrm{TE}_{m,p}$ modes. (The dashed straight line corresponds to the design C-value of 2.24 and the right vertical scale gives the cutoff frequency f_c (GHz) $= (15/\pi)\chi_{mp}/R_0$ for $R_0 = 3.36$ cm.)

soluble subject to appropriate radiation boundary conditions at the cavity ends

$$\frac{dV(z)}{dz} \mp i(4\pi^2 f^2/c^2 - k_{\perp,mp}^2)^{1/2} V(z)|_{z_{\mathrm{in}},\, z_{\mathrm{out}}} = 0. \quad (26)$$

Numerically solving (25), where $k_{\perp,mp} = \chi_{mp}/R_0(z)$ is the transverse wavenumber with $\chi_{mp}(C(z))$ obtained from the characteristic equation (9), the Q_D factor is evaluated as $Q_D = f_R/2f_I$. Taking into account the ohmic losses, which always decrease the resonant frequency, the calculated quantities to be compared with those from the experiment are $f = f_R\sqrt{1-1/Q_\Omega}$ and $Q_T = Q_D Q_\Omega/(Q_D + Q_\Omega)$ with the ohmic Q_Ω factor given by (19).

C. Comparison

To compare theory with experiment, we detected over the range 8–16 GHz all the fundamental TE modes in the corrugated cavity of Fig. 12. The dependence of $\chi_{m,p}$ on C for these modes is given by the solid line, shown in Fig. 13, where the dashed curves refer to the corresponding modes in the smooth-wall coaxial cavity. We can see that, relative to the smooth cavity, the effect of the corrugations is toward decreasing the eigenvalue $\chi_{m,p}$, and, accordingly, the cutoff frequency; nevertheless, surface $\mathrm{TE}_{m,1}$ modes with $5 \leq m \leq 9$ [see Fig. 13(a)] are essentially insensitive to the presence of the inner conductor of our 2.24-design C corrugated cavity. This is consistent with the fact that such modes are associated with the highest Q_Ω factor, as shown in Table I. On the other hand, volume modes with $m \leq 4$ [see Fig. 13(b)] are strongly affected by the corrugations, having their Q_Ω factors reduced from typical values of 12 000 (in the smooth-wall case) to 6000 $\sim$ 7000 in the corrugated cavity.

Measured resonant frequencies and Q_T factors are also given in Table I, where good agreement between theory and experiment is found, in that the magnitude of the relative error in frequency is below 0.5%. A few comments, however, are in order. First, we note that for higher frequency volume modes (>12 GHz), the measured frequency is higher than the predicted one, while the converse occurs for surface $\mathrm{TE}_{m,1}$ modes with $5 \leq m \leq 9$. On considering that surface modes are insensitive to the presence of the coaxial insert, we conjecture that the systematic positive errors associated with volume modes are due to geometrical effects of the corrugations rather than experimental uncertainties in individual measurements. This suggests that corrections should be made to the predicted frequencies of higher frequency modes. The correction may be accounted for on the basis of the effect of a finite number of slots per wavelength [7], which causes a reduction of the effective depth d. The number of slots per wavelength is determined by the frequency of operation and mechanical manufacturing restrictions, so that the present corrugated rod is contemplated with eight slots per wavelength at 16 GHz.

By a simple transmission-line analysis, it is shown [7] that on the free-space side of the corrugations, the coaxial insert appears as a corrugated surface with infinite number of slots per wavelength, but with a smaller depth d'

$$d' = d - \frac{\ln 2}{\pi} l \quad (27)$$

provided that $l \ll \lambda$, as we considered in our design. Although this result strictly applies if $R_i \gg \lambda$, measurements indicate [9] that it is valid approximately even when $R_i \geq 0.6\lambda$, such that, for the present cavity, this translates into $f \geq 12$ GHz. Thus, substituting in (27) the design values $l = 1.0$ mm, and $d = 1.5$ mm gives $d' = 1.3$ mm. Considering now the corrected corrugation parameter $d'/R_i = 0.09$ for higher frequency (>12 GHz) volume modes, the resonant frequencies and Q_T factors are recalculated and displayed in Table II. We notice that the theoretical frequencies are always higher than the experimental values (or almost coincident for $\mathrm{TE}_{3,2}$ and $\mathrm{TE}_{2,2}$ modes, shown in Table I) with a negative systematic error less than 0.5% in magnitude. As for the Q_T values, it is seen in Tables I and II that, in any event, the agreement between theory and experiment lies within experimental accuracy.

V. Conclusions

The resonant properties of gyrotron coaxial cavities with a longitudinally slotted inner cylinder were investigated on the basis of a surface impedance model with the requirement that the slot width be less than a half-wavelength of the operating TE mode. As gyrotron cavities operate near cutoff, their selective properties are mainly expressed by the dependence of the transverse eigenvalue $\chi_{m,p}$ on the coaxial C. The

TABLE I
CALCULATED AND MEASURED VALUES OF RESONANT FREQUENCIES AND Q FACTORS FOR FUNDAMENTAL TE MODES IN THE CORRUGATED COAXIAL CAVITY OF FIG. 12

$TE_{m,p}$ Mode	Calculated				Measured		Percent Error $\frac{f_{exp}-f_{theo}}{f_{theo}}$
	f [GHz]	Q_D	Q_Ω	Q_T	$f \pm 6x10^{-4}$ [GHz]	Q_T	
5,1	9.0702	760	15010	724	9.0558	717 ± 25	-0.16
6,1	10.6373	1067	15182	997	10.6168	992 ± 30	-0.19
7,1	12.1749	1447	15150	1321	12.1512	1279 ± 60	-0.19
8,1	13.6953	1858	15052	1654	13.6668	1518 ± 80	-0.21
9,1	15.2048	2332	14937	2017	15.1791	1946 ± 50	-0.17
1,2	8.3044	649	5794	584	8.2899	568 ± 40	-0.17
2,2	9.1519	790	6018	698	9.1569	706 ± 25	+0.05
3,2	10.4587	1029	6458	887	10.4659	1037 ± 90	+0.07
4,2	12.0963	1382	7200	1159	12.1169	1143 ± 100	+0.17
5,2	13.9343	1900	8340	1547	13.9700	1535 ± 70	+0.25
6,2	15.8609	2524	10064	2018	15.8928	1938 ± 100	+0.20
0,1	8.0092	604	5725	546	7.9749	514 ± 35	-0.43
0,2	15.6584	2664	7288	1951	15.7328	1873 ± 80	+0.47
1,3	15.7945	2710	7264	1974	15.8191	1948 ± 60	+0.15

TABLE II
MEASURED AND RECALCULATED VALUES OF RESONANT FREQUENCIES AND Q_T-FACTORS FOR HIGHER FREQUENCY MODES TAKING INTO ACCOUNT A REDUCED CORRUGATED DEPTH

TE Mode	Recalculated		Measured		Percent Error $\frac{f_{exp}-f_{theo}}{f_{theo}}$
	f [GHz]	Q_T	$f \pm 6 \times 10^{-4}$ [GHz]	Q_T	
4,2	12.1551	1193	12.1169	1143 ± 100	-0.31
5,2	13.9976	1588	13.9700	1535 ± 70	-0.20
6,2	15.9233	2095	15.8928	1938 ± 100	-0.20
0,2	15.7328	2008	15.7328	1873 ± 80	-0.06
1,3	15.8191	2033	15.8191	1948 ± 60	-0.38

question about how the corrugation parameters affect the shape of the $\chi_{m,p}(C)$ curves was clarified by analyzing an expression derived for the slope function $d\chi_{m,p}/dC$. It was shown that the sign of $d\chi_{m,p}/dC$ is opposite to that of the function $f(y)$—whose definition explicitly encompasses the corrugation parameters d/R_i, l/s, and the azimuthal index m of $\mathrm{TE}_{m,p}$ modes. A wealth of information about the behavior of the $\chi_{m,p}(C)$ curves is contained in this function, and a number of examples were given to illustrate its usefulness in anticipating the shape of $\chi_{m,p}(C)$ without solving the characteristic equation (9). In connection with this, it was demonstrated that, irrespective of the azimuthal index value, when $d/R_i = l/s$ the $\chi_{m,p}(C)$ curve is flat over a wide range of C, while if $d/R_i < l/s$, the $\chi_{m,p}(C)$ curve exhibits only one minimum. These peculiarities can be helpful in design methods whereby an optimum set of values for d/R_i and l/s is to be chosen to give a desired mode spectrum.

The theory was compared with experiment in which resonant frequencies and Q_T factors were measured for TE modes operating over the range 8–16 GHz in a cavity with $d/R_i = 0.10$, $l/s = 0.42$, and $N = 40$ slots. Good agreement was found in that the magnitude of the relative error in frequency is below 0.5%. Moreover, if the slot depth is corrected for higher frequency volume modes—to account for the effect of a finite number of slots—the predicted frequencies are consistently higher than the measured values within a relative error of -0.5%.

In conclusion, it follows that the surface impedance model proves to be an effective tool in the analysis of corrugated coaxial cavities. Such structures are relevant for megawatt gyrotrons where highly selective resonators are required to ensure high conversion efficiency.

As reported in recent gyrotron experiments, output powers in excess of 1 MW with conversion efficiencies on the order of 30% have been measured for high-order $\mathrm{TE}_{31,17}$ and $\mathrm{TE}_{28,16}$ modes at 165 [10] and 140 GHz [11], respectively. We stress again that a major technical restriction on the level of the radiated microwave power at long-pulse (second duration) or continuous wave (CW) operation is posed by ohmic losses in the resonator walls. For presently available cooling techniques, the ohmic heating density cannot exceed the upper limit of 3–4 kW/cm^2 and, accordingly, the RF electric-field strength inside the cavity should be typically restricted to tens of kilovolts/centimeters. According to the Kilpatrick criterion [12], the breakdown electric field at microwave frequencies as given by $E_{br}(V/m) \cong 0.8 \times 10^3 \sqrt{f(\mathrm{Hz})}$ is well above the maximum electric-field intensity ensued from ohmic heating considerations. Moreover, electrical breakdown near the sharp

edges of the corrugations is of no concern since the slot width is less than a half-wavelength of the operating mode and, in this sense, the corrugated inner conductor, being electrically smooth, is represented by a reactive surface. In addition, corrugated coaxial cavities can be useful in guided-wave applications involving filters, frequency-tunable resonators, and devices for analyzing the modal composition of a signal.

REFERENCES

[1] K. E. Kreischer, R. J. Temkin, H. R. Fetterman, and W. J. Mulligan, "Multimode oscillation and mode competition in high-frequency gyrotrons," *IEEE Trans. Microwave Theory Tech.*, vol. MTT-32, pp. 481–490, May 1984.

[2] M. Makowski, "ECRF systems for ITER," *IEEE Trans. Plasma Sci.*, vol. 24, pp. 1023–1032, June 1996.

[3] J. J. Barroso, P. J. Castro, and R. A. Corrêa, "Geometrical effects in gyrotron coaxial cavities: Application to mode selection," *IEEE Trans. Microwave Theory Tech.*, vol. 43, pp. 1384–1386, June 1995.

[4] G. S. Nusinovich, M. E. Read, O. Dumbrajs, and K. E. Kreischer, "Theory of gyrotrons with coaxial resonators," *IEEE Trans. Electron Devices*, vol. 41, pp. 433–438, Mar. 1994.

[5] C. T. Iatrou, S. Kern, and A. B. Pavelyev, "Coaxial cavities with corrugated inner conductor for gyrotrons," *IEEE Trans. Microwave Theory Tech.*, vol. 44, pp. 56–64, Jan. 1996.

[6] C. T. Iatrou, "Mode selective properties of coaxial gyrotron resonators," *IEEE Trans. Plasma Sci.*, vol. 24, pp. 596–605, June 1996.

[7] R. E. Collin, *Field Theory of Guided Waves.* New York: McGraw-Hill, 1960, ch. 11.

[8] T. B. A. Senior and J. L. Volakis, "Generalized impedance boundary conditions in scattering," *Proc. IEEE*, vol. 79, pp. 1413–1420, Oct. 1991.

[9] C. Dragone, "Reflection, transmission, and mode conversion in a corrugated feed," *Bell Syst. Tech. J.*, vol. 56, pp. 835–867, 1977.

[10] C. T. Iatrou, O. Braz, G. Dammertz, S. Kern, M. Kuntze, B. Piosczyk, and M. Thumm, "Design and experimental operation of a 165-GHz, 1.5-MW, coaxial-cavity gyrotron with axial RF output," *IEEE Trans. Plasma Sci.*, vol. 25, pp. 470–479, June 1997.

[11] B. Piosczyk, O. Braz, G. Dammertz, C. T. Iatrou, S. Kern, M. Kuntze, A. Möbius, M. Thumm, V. A. Flyagin, V. I. Khishnyak, V. I. Malygin, A. B. Pavelyev, and V. E. Zapevalov, "A 1.5-MW, 140-GHz, $\mathrm{TE}_{28,16}$ coaxial cavity gyrotron," *IEEE Trans. Plasma Sci.*, vol. 25, pp. 460–469, June 1997.

[12] W. D. Kilpatrick, "Criterion for vacuum sparking designed to include both RF and DC," *Rev. Sci. Instrum.*, vol. 28, pp. 824–826, 1957.

Joaquim J. Barroso received the B.S. degree in electrical engineering and the M.S. degree in plasma physics from the Technological Institute of Aeronautics, São José dos Campos, Brazil, in 1976 and 1980, respectively, and the Doctor degree in plasma physics from the National Institute for Space Research (INPE), São Paulo, Brazil, in 1988.

He has been with INPE since 1982, where he has been involved in the design and construction of a high-power 32-GHz gyrotron, which became operational in 1993. From 1989 to 1990, he was a Visiting Scientist at the Plasma Fusion Center, Massachusetts Institute of Technology. His current interests include high-power microwave generators and plasma technology.

Rafael A. Corrêa received the B.S. degree in physics from the University of São Paulo, São Paulo, Brazil, in 1978, the M.S. degree from the National Institute for Space Research (INPE), São Paulo, Brazil, in 1983, and the Doctor degree in plasma physics from the Technological Institute of Aeronautics, São José dos Campos, Brazil, in 1993.

He has been with the INPE since 1979, and, in 1982, joined the Laboratory of Plasma. From 1994 to 1995, he was a Visiting Scientist at the Institute for Plasma Research, University of Maryland at College Park. His research interests are in gyrotrons, free electron lasers, and plasma physics.

Pedro José de Castro received the B.S. and M.S. degrees in radiophysics from the People's Friendship University, Moscow, Russia, in 1978 and 1980, respectively, and the Doctor degree in electrical engineering from the University of São Paulo, São Paulo, Brazil, in 1989.

Since 1986, he has been with the National Institute for Space Research (INPE), São Paulo, Brazil, where he has been involved in the operation of a 32-GHz gyrotron. His current research interests are microwave measurement techniques and vacuum technology.

Dr. de Castro is a member of the Brazilian Microwave Society.